
Proceedings Paper:
Malendowski, M., Burgess, I. orcid.org/0000-0001-9348-2915 and Glema, A. (2017) 03.07: Robustness in fire of a new type of beam-to-column connection. In: Ce/Papers. Eurosteel 2017, 13-15 Sep 2017, Copenhagen, Denmark. Ernst & Sohn Verlag , pp. 550-559.

https://doi.org/10.1002/cepa.92

---

ce/papers
The online collection for conference papers in civil engineering
Ernst & Sohn A Wiley Brand

EUROSTEEL 2017, September 13–15, 2017, Copenhagen, Denmark

Robustness in fire of a new type of beam-to-column connection

Michał Malendowski*,[a], Ian Burgess[b], Adam Glema[a]

[a]Poznan University of Technology, Institute of Structural Engieenering, Poland
michal.malendowski@put.poznan.pl, adam.glema@put.poznan.pl
[b] University of Sheffield, United Kingdom
ian.burgess@sheffield.ac.uk

ABSTRACT

In this paper a new type of beam-to-column connection is introduced, which is capable of absorbing both very large rotations and axial movements, due firstly to thermal elongation and subsequently to extreme weakening of the connected beam. The main idea is to connect the beam and column using a special connector bolted to the column flange using a face-plate and to the beam web using a fin-plate. Between these a highly ductile element, which is in this case a hollow circular tube, is included. This plays the crucial role in absorbing beam-end movements occurring firstly during the expansion of the beam and secondly during its catenary behaviour at very high temperatures.
This study aims to extend the research on this connection to structural case studies in the context of performance-based structural fire engineering design. The connection has been modelled using different approaches, starting with 3-D finite element modelling and proceeding to validated simplifications which feed into a component-based model. In order to make calculations feasible, the mathematical model of the ductile component is developed and calibrated using the information provided by parametrized numerical FEM computations. The component model is developed to be capable of representing the hysteresis occurring due to deformation-reversals as temperatures rise, as well as failure corresponding to fracture in tension. Thus, the component model is described as a function of displacement and temperature, including sufficiently realistic plastic deformation and fracture criteria. This model is then implemented into global FEM models and utilized to assemble the stiffness matrix of a special connector element used to join the beam and column nodes. This component-based connection model is then applied in some comparative studies.

Keywords: Steel frames, connections, fire, ductility

1 INTRODUCTION

In this paper a new type of beam-to-column connection is introduced. The need to develop a connection which can accommodate the significant simultaneous rotations and axial elongations occurring in fire was initially illustrated in full scale fire tests such as those at Cardington, and subsequently by the total collapse of the "7 World Trade" building during the events of 11 September 2001. In the latter case the inability of traditional bolted beam-to-column connections to deal with the axial expansion of beams was held [1-2] to be responsible for the connection fractures which initiated the progressive collapse sequence. For this reason a special connection, capable of absorbing both very large rotations and axial movements, due firstly to thermal elongation and subsequently to extreme weakening of the connected beam, is proposed. The main idea is to connect the beam and column using a special connector bolted to the column flange using a face-plate and to the beam web using a fin-plate. Between these a highly ductile element, which is at this stage a hollow circular tube, is included. Scaled prototypes of this connection have been manufactured at the University of Sheffield, using 3-D printing technology, and tested for suitability [3-4].
This study aims to extend this research to structural case studies in the context of performance-based structural fire engineering design. The connection has been modelled using different approaches, starting with 3-D finite element modelling and proceeding to validated simplifications which feed into a component-based connection model. In order to make calculations feasible, the

mathematical model of the ductile component is developed and calibrated using the information provided by parametrized numerical FEM computations. The model is developed to be capable of representing the hysteresis occurring due to deformation-reversal as temperatures rise, as well as failure corresponding to fracture in tension. Thus, the component model is described as a function of displacement and temperature, including sufficiently realistic plastic deformation and fracture criteria. This model is implemented in global FEM models and used to assemble the stiffness matrix of a special connector element which joins the beam-end and column nodes. This component-based connection model is then used in comparative studies.

2 CONNECTION SCHEME

The scheme of the proposed connection is shown in Fig.1, with the parameters necessary to describe its behaviour marked. The beam is connected to column flange using the new connector, in which the cylindrical motion-absorber made of hollow circular tube plays the crucial role. The performance of this absorber when simultaneous large deformations, both axial and rotational, occur at high fire temperatures is of particular interest in this research.

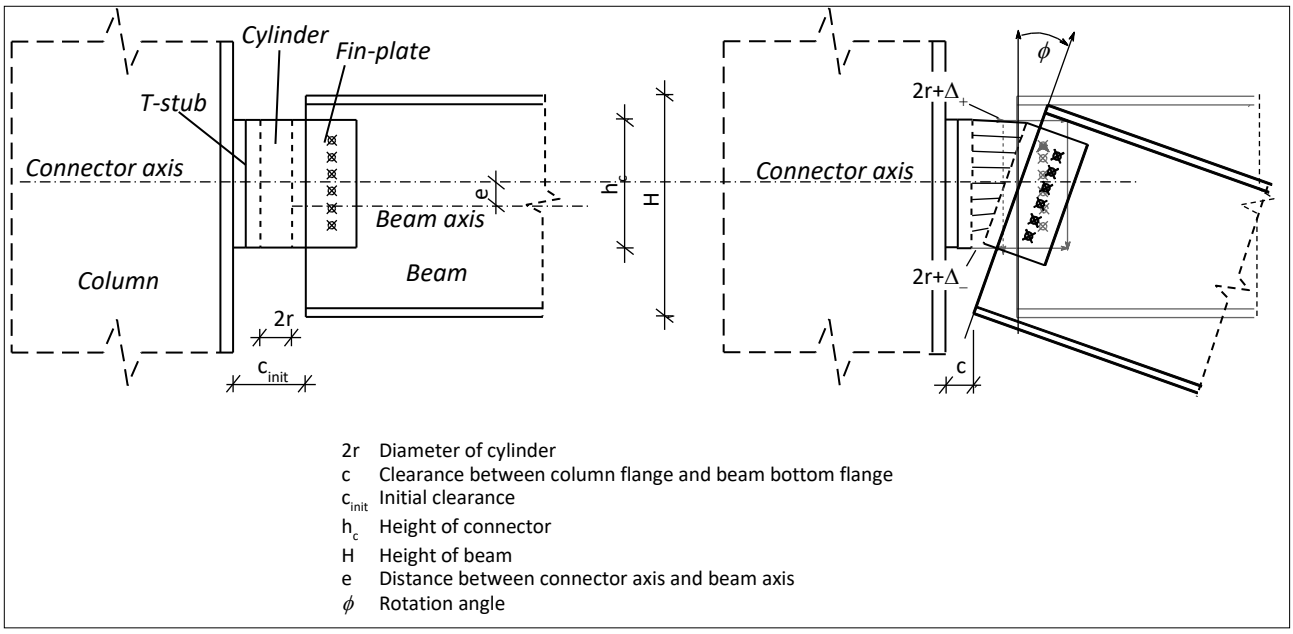

Fig. 1. Schematic draw of proposed connection.

3 PRELIMINARY EXPERIMENTAL AND NUMERICAL STUDIES

In [3] Briggs conducted experimental investigations of the performance of prototypes of this connection made of 316L stainless steel, manufactured at the University of Sheffield using 3-D printing technology. In parallel Pimblett [4] had conducted preliminary numerical and analytical studies on this connection, aiming to investigate its potential usage for improved structural robustness. The promising results of those two works resulted in a continuation of this research, of which this work is part. The experimental results obtained in [3] form the basis for verification of numerical models which are further used to calibrate the mathematical model of a component. These experimental results will be shown in the model verifications of Section 5.

4 MATHEMATICAL MODEL OF THE DUCTILE CONNECTION COMPONENT

4.1 Behaviour of component

The proposed mathematical model is based on observation of the component's force-displacement relationship under cyclic compression and tension. The characteristic behaviour observed, both in experimental and numerical tests, leads to two basic assumptions underpinning the development of the mathematical model of the force-displacement relationship. Firstly, it can be seen that the initial plastic mechanisms in either tension or compression (following the brief elasto-plastic phase) on the test force-displacement graphs in Fig. 2(b) occur at almost identical force values. This implies that, for both tension and compression, the yield loci shown in Fig. 2(a) can be described by identical formulas. The second observation is that the relationship between the resistance of the component and the component deformation converges to the same yield locus at large deformations, regardless of the number of preceding cycles. This is valid both for compression and tension. Hence, in order to find the parameters of any model describing the yield line under cyclic loading, it is sufficient to do separate tests in tension and compression, and to use this data to feed the mathematical expression. These principles are shown in Fig.2, but will also be observed in further verification and validation graphs concerning particular component examples.

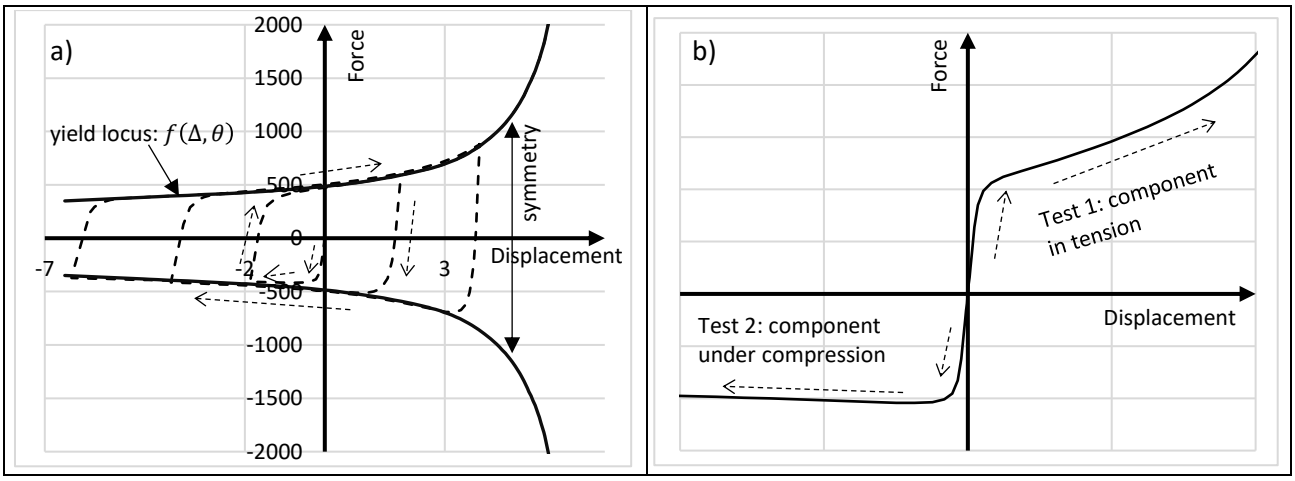

Fig. 2. Observed behaviour of connection component: a) in cyclic testing, b) in separate tension and compression tests.

4.2 Model of force-displacement relationship

In accordance with these principles, the authors propose to describe a rigid-plastic yield locus by an analytical function that best fits the actual yield lines observed during tests. As a result, the relationship between the resistance of the component (force) and its axial elongation will be expressed in the following iterative manner:

$$F^{i+1}(\Delta,\theta)=\begin{cases} F^{i}+k.\delta\Delta & \text{if} \quad F^{i}+k.\delta\Delta \le f(\Delta,\theta) \\ f(\Delta,\theta) & \text{otherwise} \end{cases} \tag{1}$$

where F^{i+1} is the force at the step $i+1$ of the iteration, Δ is the total elongation (or contraction) of the component, $\delta\Delta$ is the displacement increment, k is the appropriate tangent stiffness and θ is the temperature. The yield locus is defined by the function $f(\Delta,\theta)$. The tangent stiffness of the component must maintain the following relationship:

$$k=\max\begin{cases} k_{init} \\ \dfrac{\partial f(\Delta,\theta)}{\partial\Delta} \end{cases} \tag{2}$$

in which k_{init} is the initial stiffness obtained from tests. Additionally, the final stiffness k is reduced two times when the component is tensioned from compressed state ($\delta\Delta > 0$ and $\Delta < 0$). This is due to experimentally observed behaviour, both in numerical and real tests.
The yield function depends on the yield stress of the material, which is temperature-dependent, and on the four additional parameters: a, b, c, d, which depend only on the geometry of the component. Finally the yield function takes the form:

$$f\left(\Delta,\theta\right)=\frac{k_{y,\theta}.a}{\left(\Delta/2-b\right)^{2}+1}.\exp\left(c.\frac{\Delta}{2}\right)+k_{y,\theta}.d \tag{3}$$

It can be seen that the displacement and temperature fields are decoupled, so the parameters a, b, c, and d can be obtained from separate tests at different temperatures. Temperature dependence is entirely within the yield reduction factor ($k_{y,\theta}$). Generally, parameters a, b, c and d are independent of temperature and are derived using nonlinear best-fit curve approximations. Nonetheless, tests show that values of these parameters can slightly differ with respect to best fit at different temperatures. These differences are so small that their values can be taken as a single average from the best-fit values at different temperatures, without loss of accuracy.

4.3 Fracture criterion

In general the failure elongation of the component should be based on laboratory tests. But for the sake of simplicity the EN 1993-1-2 [5] ultimate limiting strain $\varepsilon_{t,\theta}=0.15$ is used, regardless of the temperature. This limiting strain is then used to calculate the failure elongation using a simple one-dimensional relationship. After complete stretching the modelled component becomes effectively flat (Fig.3.), and may be considered as a simple tensile specimen. Thus, failure is considered to occur at the limiting elongation of the component, calculated using the formula:

$$F\left(\Delta,\theta\right)=\begin{cases}F\left(\Delta,\theta\right) & \text{if} \quad \Delta\le\left(\pi-2\right)\left(1+\varepsilon_{t,\theta}\right)r\\ 0 & \text{otherwise}\end{cases} \tag{4}$$

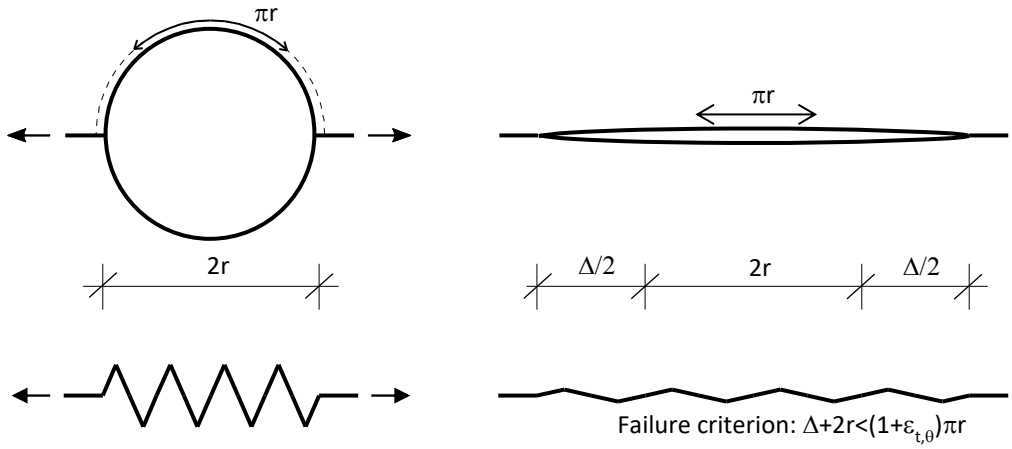

Fig. 3. Derivation of failure elongation of component.

5 VERIFICATION AND VALIDATION OF COMPONENT MODEL

The basic data for verification and validation of the component model come from the experimental tests performed by Briggs [4] and numerical computations utilizing a 3D FE model of a distorted cylinder using shell elements. Because the experimentally investigated component was made of 316L stainless steel, for numerical modelling the material parameters at elevated temperatures were taken from work by Brnic [6] and Wilkinson [7]. The Briggs experiments consisted of 4 cyclic compression-tension tests at ambient temperature and 4 compression tests at elevated temperatures. The full list of these tests is given in Table 1.

Table 1. List of experimental tests on the component [4]

Name:	Strip 2A	Strip 2B	Strip 2C	Strip 2D	Strip 3A	Strip 3B	Strip 3C	Strip 3D
Loading type	cyclic	cyclic	cyclic	cyclic	compressed	compressed	compressed	compressed
Temperature	20°C	20°C	20°C	20°C	350°C	450°C	550°C	650°C

The experimental and numerical results are presented in Figs. 4 and 5. The material parameters given by Brnic give a close correspondence with experimental results, except that the yield stress values at elevated temperatures given by Brnic seem underestimated compared to the results obtained by Briggs in his experimental work on the connection components (Fig.5: Strip 3D). Because of the limitation on length of this paper, only selected results are shown here; the graphs are selected to show the best and worst correspondence between experiments and simulations.

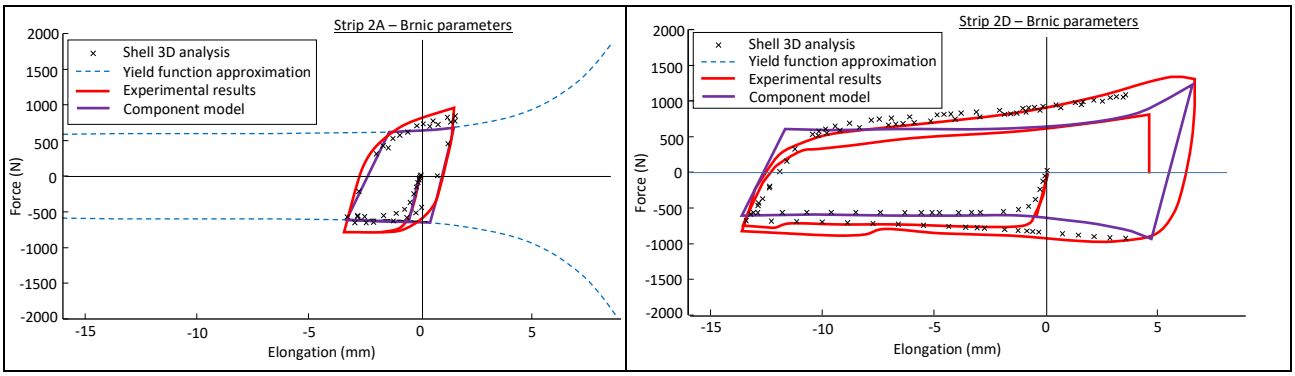

Fig. 4. Comparison between experimental results, numerical results and the component model for a component under cyclic loading at ambient temperature.

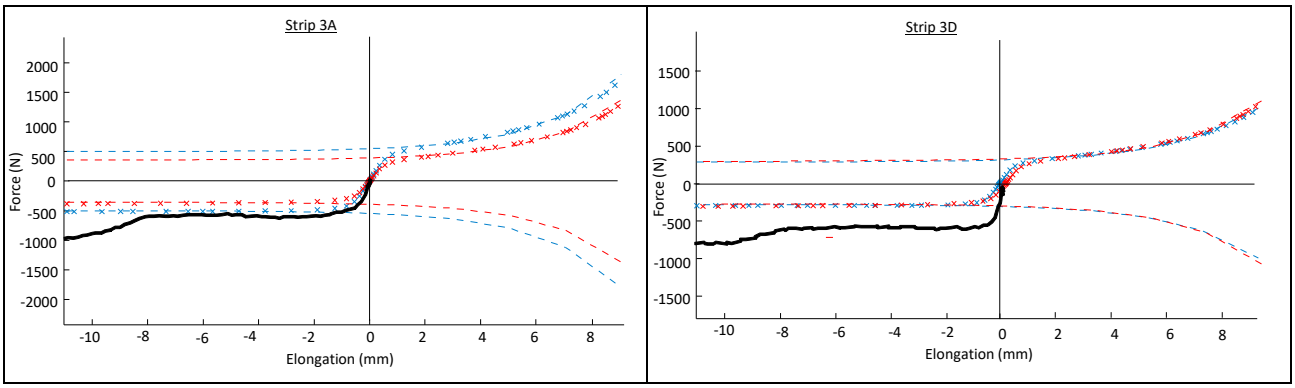

Fig. 5. Comparison between experimental results, numerical results and the component model for a component under compression at 350°C (Strip 3A) and 650°C (Strip 3D).

6 CALIBRATION OF COMPONENT MODEL

In order to obtain optimum values of the parameters in the proposed mathematical model, a series of numerical tests were carried out. Several separate compression and tension tests of the 3D shell element model of a single component were conducted at different temperatures. The resulting force-displacement relationships were then combined and processed. Finally the a, b, c and d parameters of the yield function and the initial stiffness of the spring, k_{init}, were derived. The way in which these parameters were derived, based on simple tension and compression tests, is shown in Fig.6. The best-fit parameters are based on optimization of the curve-fit, using the "trust-region-reflective" algorithm, which is available in the Matlab environment [8]. The parameters are then averaged for any particular geometry, in order to decouple the geometry and temperature fields. Comparative studies were carefully conducted, to ensure that averaging the values of model parameters from tests at different temperatures does not introduce significant errors in solution. Examples are compared in Fig.7.

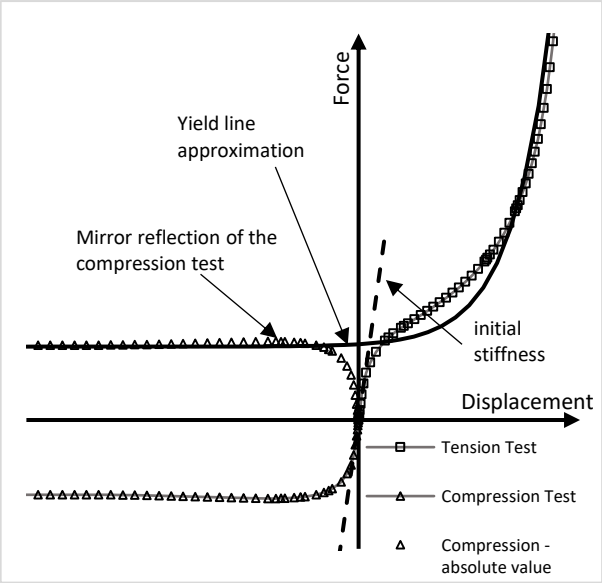

Fig. 6. Method for deriving parameters of mathematical model of the component.

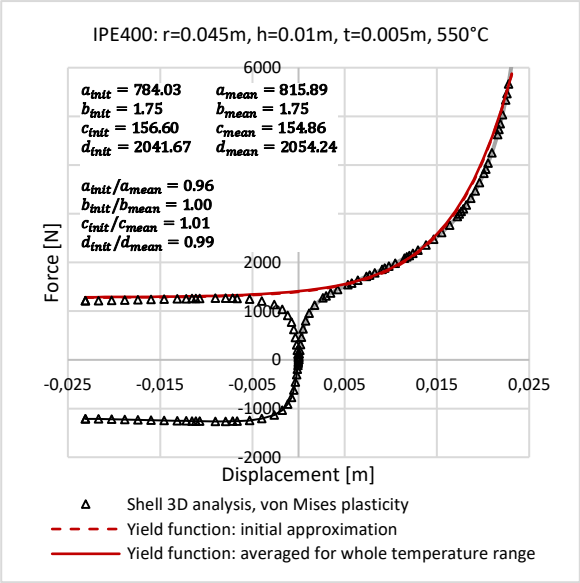

Fig. 7. Example of comparative graph for derivation of model parameters.

With the parameters k_{init}, a, b, c and d derived for each geometry, the studies focused on the relationship between the geometrical parameters of a component and the parameters of the yield function. In total 24x4 geometries have been chosen, based on connecting beams of IPE section varying from 300-600 mm in height. This finally resulted in 2016 cases being tested, subjecting each geometry to temperatures from 20°C to 1100°C. The basic material parameters were for S355 steel with Eurocode material parameters; final values of the yield model parameters are obtained from the formulae given in (5).

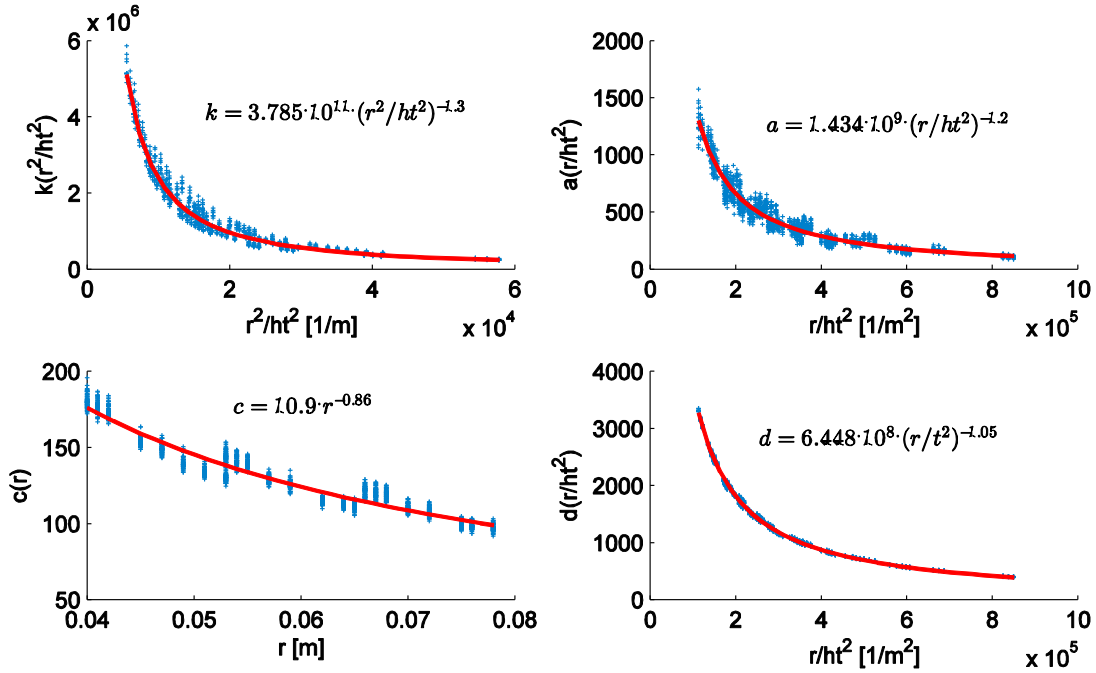

Fig. 8. The best-fit curves together with test data for yield model parameters.

$$\begin{cases} k_{init} = 3.785 \cdot (r^2/ht^2)^{-1.3} \cdot 10^{11} \\ a = 1.434 \cdot (r/ht^2)^{-1.2} \cdot 10^{9} \\ b = 1.76 \\ c = 1.090 \cdot r^{-0.86} \cdot 10^{1} \\ d = 6.448 \cdot (r/ht^2)^{-1.05} \cdot 10^{8} \end{cases} . \quad (5)$$

in which r is cylinder radius, h is component width and t is the thickness of the tube. These relationships are again derived using the best-fit optimization as previously. The best-fit curves are shown in Fig.8 together with test data.

7 FINAL ASSEMBLY AND PERFORMANCE CHECK ON BEAM SUPPORTED BY THE PROPOSED CONNECTION

The cylinder is modelled using a set of parallel horizontal springs which together define its behaviour under axial tension/compression and bending, and one vertical spring transferring the vertical shear force through the cylinder axis (Fig. 9). The horizontal springs utilize the developed model, while the vertical spring is modelled as a standard truss element with predefined area and isotropic steel properties with von Mises plasticity. The developed component model of cylinder, being the most crucial part of the proposed connector, is utilized in a full model of a beam supported at both ends by these connectors. The mechanical model of the system being considered is shown in Fig.10, while the close-up of the connector is given in Fig.11.

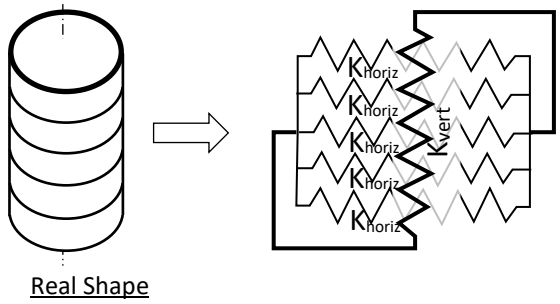

Fig. 9. Assembled cylinder model.

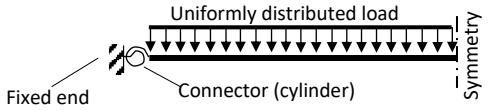

Fig. 10. Mechanical model of analysed system.

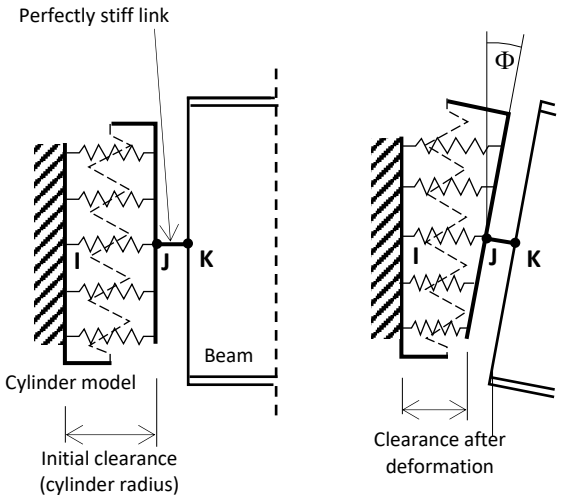

Fig. 11. Close-up of the connector in mechanical model

Three tests were used to test the performance of the proposed connection. All the examples were designed as simply supported beams according to Eurocode rules. The beams were intended to support a concrete pre-tensioned hollow-core slab floor. The assumed load category D results in a characteristic imposed load of 16 kN/m, while the dead load is 11.34 kN/m. The most severe load combination in the ULS condition gave a total uniformly distributed load equal to 37.03 kN/m, which resulted in the selection of an HEA 340 cross-section for beams of 8 m span. In the Fire Limit State the total load is reduced according to the accidental combination of actions, and was equal to 22.12 kN/m. This value of equally distributed load is taken for further analyses of beam at elevated temperatures. The list of tests and their parameters is given in Table 2; the critical temperatures of beams, according to EC calculations, are in the range 580°C -600°C for all cases.

Table 2. List of numerical examples of beam supported by proposed connection.

		Beam length (L)	Section height (Hb)	Flange width (B)	Flange thickness (tf)	Web thickness (tw)	Cylinder height (H = 0.7Hb)	Cylinder wall thickness (t = 0.5tw)	Cylinder radius (r)
	Section	[m]	[mm]	[mm]	[mm]	[mm]	[mm]	[mm]	[mm]
TEST-1	HEA 340	8.00	330	300	16.5	9.5	231	4.75	28.28
TEST-2	IPE 300	4.00	300	150	10.7	7.1	210	3.55	28.04
TEST-3	IPE 450	6.00	450	190	14.6	9.4	315	4.7	28.16

8 RESULTS

The performance analyses of the connection are checked using both the proposed model and a full 3D model of the cylinder composed of shell finite elements. The beam is modelled in both cases using beam elements, integrated at each increment of the analysis. The comparative results for tests 1-3 (Tables 2 and 3) are shown in Figs. 12-17. All tests are performed using the Abaqus Standard iterative solver [9], which required creation of a Fortran user subroutine introducing the developed model as a separate, two-noded non-linear spring finite element.

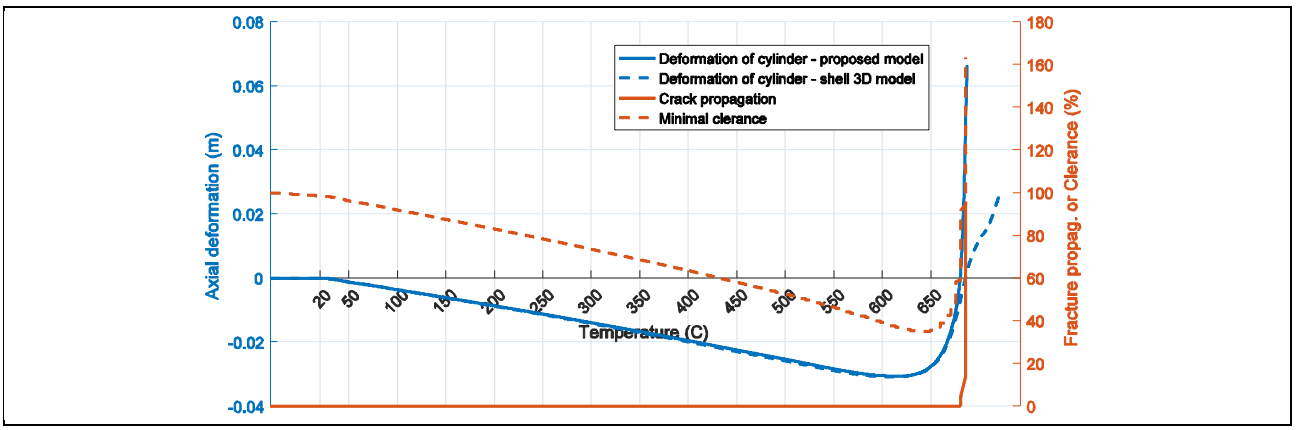

Fig. 12. TEST-1: relationship between the temperature and axial deformation of cylinder compared with the information about minimal clearance and crack propagation.

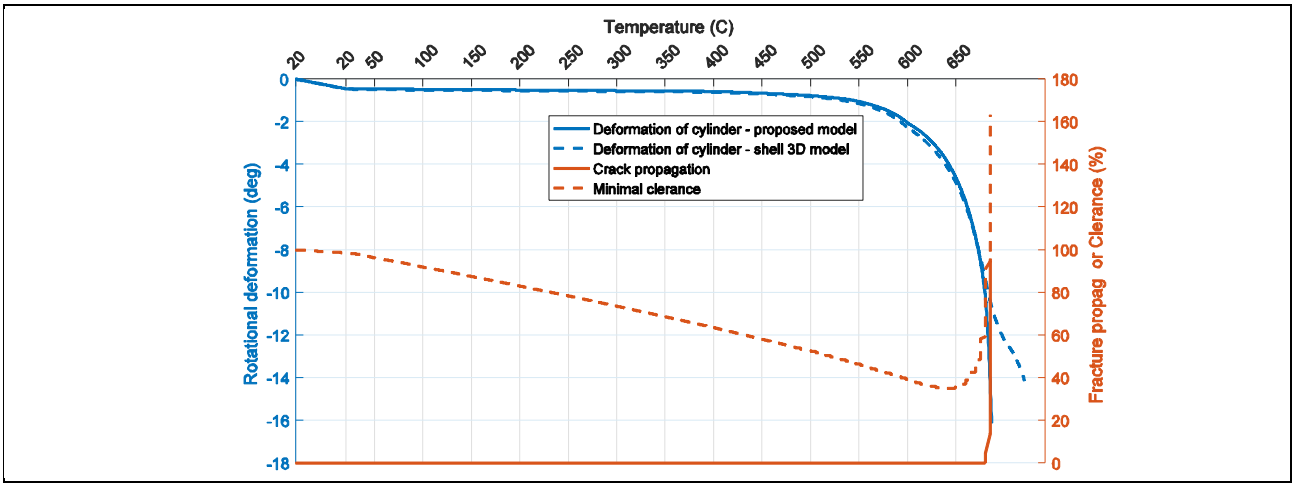

Fig. 13. TEST-1: relationship between the temperature and rotation of cylinder's right end compared with the information about minimal clearance and crack propagation.

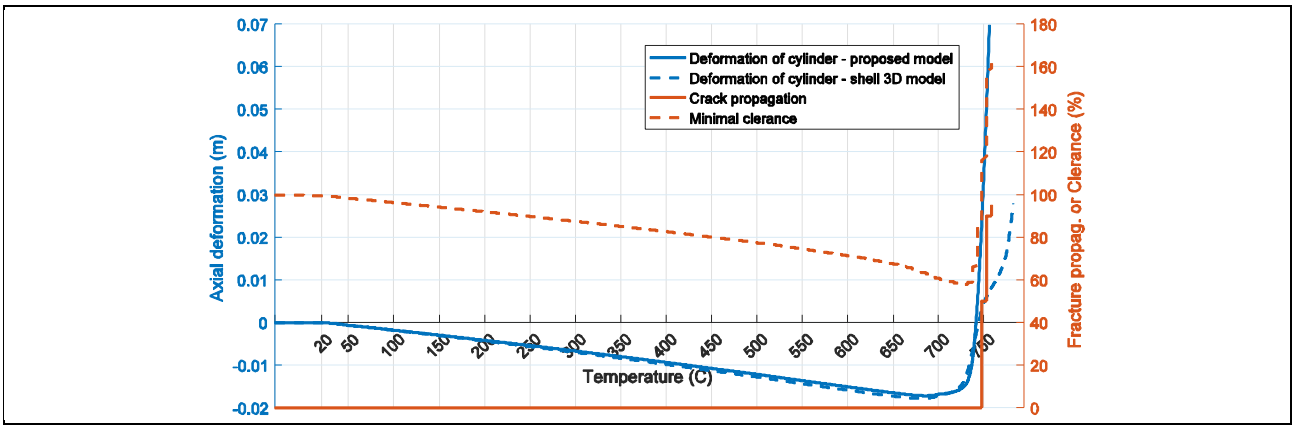

Fig. 14. TEST-2: relationship between the temperature and axial deformation of cylinder compared with the information about minimal clearance and crack propagation.

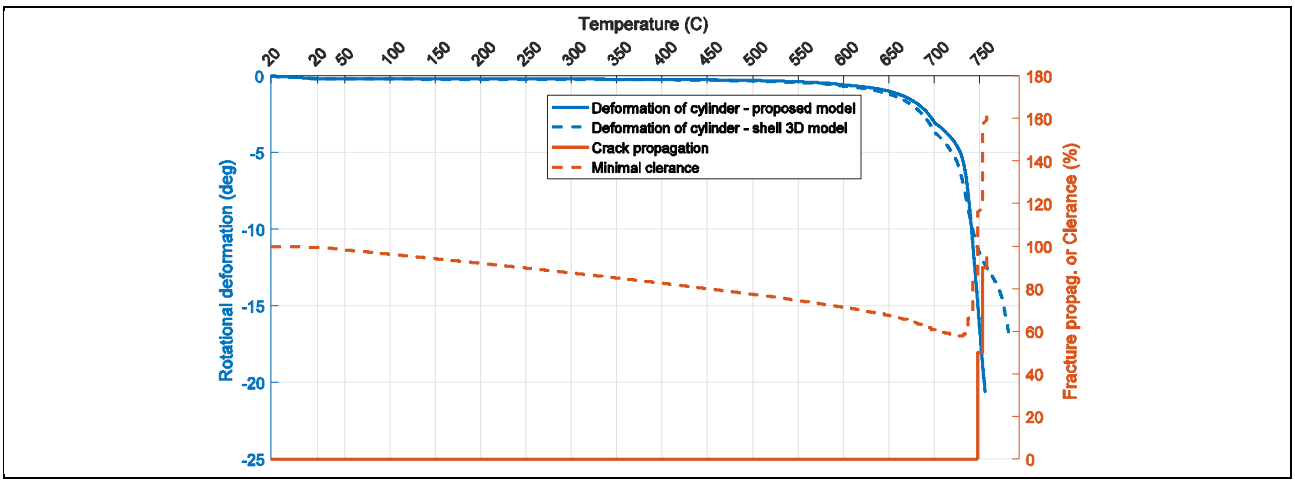

Fig. 15. TEST-2: relationship between the temperature and rotation of cylinder's right end compared with the information about minimal clearance and crack propagation.

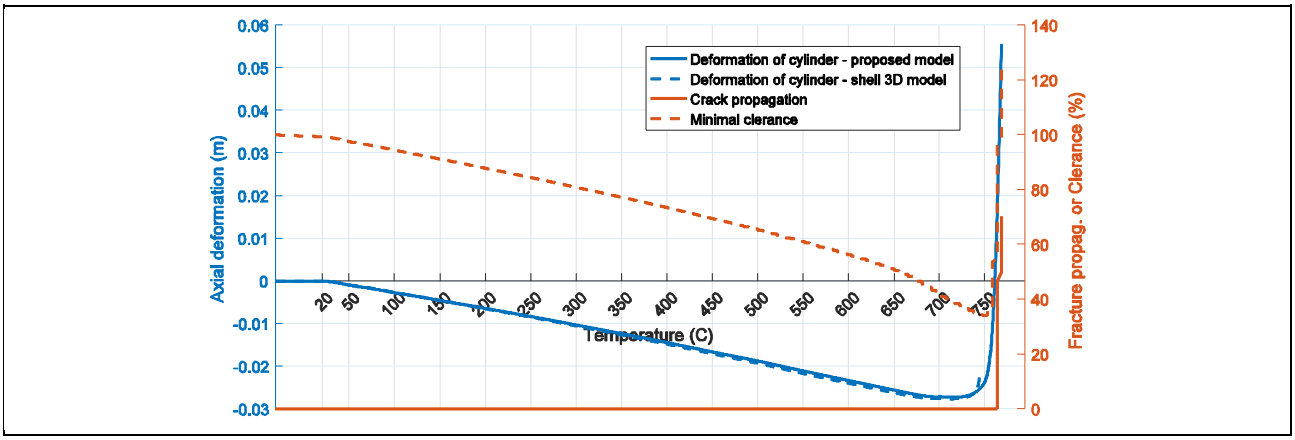

Fig. 16. TEST-3: relationship between the temperature and axial deformation of cylinder compared with the information about minimal clearance and crack propagation.

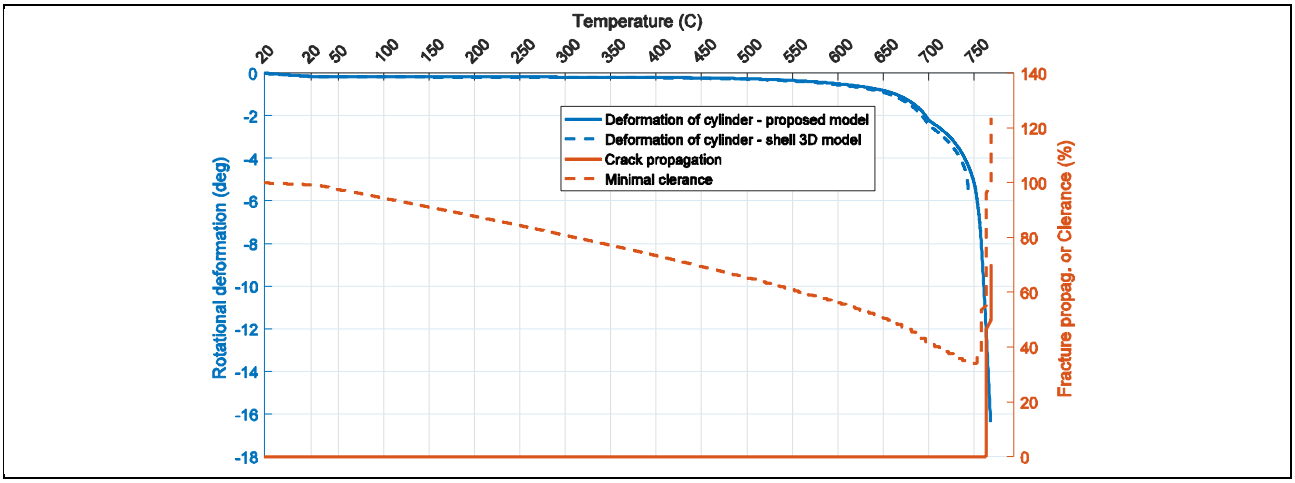

Fig. 17. TEST-3: relationship between the temperature and rotation of cylinder's right end compared with the information about minimal clearance and crack propagation.

9 FINAL REMARKS AND CONCLUSIONS

1. The component model has been verified and validated against existing experimental results and numerical tests. Because of the currently limited number of experiments, some additional experimental work is required.

2. The model is temperature-dependent and the parameters are generalized using closed-form equations based on the relationship between parameters and the actual dimensions of a component. Hence, there is no need to calibrate model parameters each time the geometrical dimensions change.
3. The assembled connection, using the developed component model, converges with the full 3D approach up to the point at which fracture occurs; this cannot be captured by standard shell element models.
4. The test examples of beams supported using this connection show that the connector efficiently absorbs both very large rotations and axial movements, due firstly to thermal elongation and subsequently to extreme weakening of the connected beam.
5. It can be seen that the connector's ability to absorb these movements is utilized by about 40% in TEST-2, and this is raised to 65% in TEST-1 and TEST-3 (see the "minimal clearance" curve in the figures above). Hence, there is still a need to develop design recommendations so that designers can optimize the dimensions of a connector with respect to beam length, beam section height and web thickness.

10 ACKNOWLEDGMENT

This research was supported in part by PL-Grid Infrastructure.

REFERENCES

[1] Wang Y.C. "An analysis of the global structural behaviour of the Cardington steel-framed building during the two BRE fire tests", Engineering Structures, Volume 22, Issue 5, pp.401-412, 2000

[2] Usmani A.S., Chung Y.C., Torero J.L., "How did the WTC towers collapse: a new theory", Fire Safety Journal, Volume 38, Issue 6, pp. 501-533, 2003

[3] Pimblett N. "Investigation a proposed connection detail for improved structural robustness", CIV4000 Final year project, The University of Sheffield, 2016

[4] Briggs J. "Experimental investigation of the performance of a modified 3D printed 316L stainless steel structural connection at elevated temperatures", CIV4000 Final Report, The University of Sheffield, 2016

[5] Eurocode 3: Design of steel structures. Part 1.2: General rules. Structural fire design. Brussels, 2005.

[6] Brnic J., Niu J., Canadija M., Turkalj G., Lanc D. „Behaviour of AISI 316L Steel Subjected to Uniaxial State of Stress at Elevated Temperatures", Journal of Materials Science and Technology, Volume 25, Issue 2, pp. 175-180, 2009

[7] Wilkinson H. "Catastrophic Fire-Testing of 3D Printed Stainless Steel", CIV4001 Final Report, The University of Sheffield, 2015

[8] MATLAB 2016a, The MathWorks Inc., Natick, MA, 2016

[9] ABAQUS 6.14-2, Dassault Systèmes, 2016